

## DEFORMATION-PROMOTED DEFECTS AND RETROGRADE CHLORITIZATION OF BIOTITE IN SLATES FROM A SHEAR ZONE, SOUTHERN IBERIAN MASSIF, SE SPAIN

JUAN JIMÉNEZ-MILLÁN<sup>1,\*</sup>, MERCEDES VÁZQUEZ<sup>2</sup> AND NICOLÁS VELILLA<sup>3</sup>

<sup>1</sup> Departamento de Geología, Universidad de Jaén, Campus Universitario, Edificio B-3, 23071 Jaén, Spain

<sup>2</sup> Departamento de Geociencias, Universidade de Aveiro, Campus Universitário, Aveiro, 3810-193, Portugal

<sup>3</sup> Departamento de Mineralogía y Petrología, Universidad de Granada, Facultad de Ciencias, Avda. Fuentenueva s/n, 18002 Granada, Spain

**Abstract**—Naturally deformed biotite in contact-metamorphosed slates affected by a shear zone of the Southern Iberian Massif near Jaén (SE Spain) were studied by X-ray diffraction, optical microscopy, scanning electron microscopy, electron probe microanalysis and high-resolution transmission and analytical electron microscopy. Biotite is found in the contact metamorphism aureole produced by the intrusion of a granodioritic stock, but shear strain caused its deformation. The southern part of the shear band is strongly deformed, containing thick clay gouge zones. The northern part is less deformed and develops weaker planar-linear fabrics. X-ray diffraction data reveal the predominance of the  $2M_1$  biotite in the undeformed samples whereas the  $1M$  polytype is predominant in the sheared samples. Chemical data and electron images of the biotite from unsheared slates do not show the presence of intercalated phases. This biotite is almost defect-free and electron diffraction patterns have sharp reflections indicating a two-layer polytype (probably  $2M_1$ ). Back-scattered electron images from the deformed biotite in the moderate deformation part of the shear zone do not reveal intergrown minerals, but the electron microprobe analyses show some Fe- and Mg-enriched compositions. Transmission electron microscopy indicates that disordered polytype packets are predominant (probably  $1M_d$ ). Their electron diffraction patterns have diffuse streaking along  $c^*$ . These packets have high dislocation densities, microcavities with  $\sim 5$  Å lattice-fringe regions (probably brucite-like sheets) and interlayering of chlorite-berthierine. Kaolinized biotite can be observed in the clay gouges from the strongly deformed south part of the shear zone. The degree of streaking, as an indication of the intensity of deformation, revealed that the disordered polytype packets are more deformed than the two-layer polytype packets. The microcavities of the disordered polytype packets could act as potential channels for transport of fluids during the shearing stage and serve as sites for chloritization of biotite, producing chlorite-berthierine domains within biotite. Berthierine is an intermediate metastable phase replaced by chlorite with along-layer transitions.

**Key Words**—Berthierine, Biotite, Chlorite, Deformation, Dislocations, Shear Zone, Iberian Massif.

### INTRODUCTION

Relatively small shear stresses are required for the onset of plastic deformation in biotite, which is ultimately produced by dislocation glide in the (001) basal planes of crystals, regardless of the orientation of compressional axes. Previous work concerning the effect of strain on biotite has been performed on samples that were deformed under laboratory conditions (*i.e.* Kronenberg, 1990; Christoffersen and Kronenberg, 1993; Noe *et al.*, 1999) or natural processes (Olives *et al.*, 1983; Sánchez-Navas and Galindo-Zaldivar, 1993; Ooteman *et al.*, 2003). High-resolution transmission electron microscopy (HRTEM) is especially useful to investigate the transformation of sheet silicates and the chloritization of biotite. 14 Å chlorite-like structure in

biotite has been interpreted to form via the replacement of K interlayer sheets by brucite-like sheets (Iijima and Zhu, 1982; Olives *et al.*, 1983; Olives and Amouric, 1983), the removal of two K interlayer sheets and two tetrahedral sheets (Veblen and Ferry, 1983) or the formation of one serpentine layer (berthierine) via loss of a K interlayer and a tetrahedral sheet (Kogure and Banfield, 2000). Based on layer sequences of interstratified chlorite-berthierine, Xu and Veblen (1996) concluded that berthierine can be considered a polymorph of the Fe-rich chlorite mineral, chamosite, with berthierine as the low-temperature phase.

In this study, naturally deformed biotite crystals in slates from a shear zone of the Southern Iberian Massif (SE Spain) were examined to investigate the influence of deformation on the presence of defects. We have also studied its influence on the polytype and the extent of stacking disorder and the formation of intercalated phases (brucite, berthierine and chlorite layers) into biotite that produce compositional modifications resulting in a non-stoichiometric behavior.

\* E-mail address of corresponding author:  
jmillan@ujaen.es  
DOI: 10.1346/CCMN.2007.0550305

## ANALYTICAL METHODS

Samples were studied using optical microscopy, scanning electron microscopy (SEM) with energy-dispersive X-ray (EDX) microanalysis, electron microprobe analysis (EMPA) and high-resolution transmission and analytical electron microscopy (HRTEM-AEM). X-ray diffraction (XRD) data were obtained with a Siemens D-5000 diffractometer using CoK $\alpha$  radiation and an Fe filter for powders of randomly oriented crystals and CuK $\alpha$  radiation and a Ni filter radiation for oriented aggregates (Universidad de Jaén). Ethylene glycolation and heat treatments were performed. The SEM study was made on polished samples with a Jeol 5800 electron microscope equipped with a Link Isis microanalyzer at 20 kV (Universidad de Jaén); observations were made using secondary and backscattered electron images in the atomic number contrast mode. The minerals were analyzed with a Camebax SX-50 automated electron microprobe (Universidad de Granada) in the wavelength-dispersive mode under the following conditions: accelerating voltage 20 kV; probe current 5 nA; electron beam diameter 0.5  $\mu\text{m}$ . The following compounds were used as standards: albite, orthoclase, periclase, wollastonite and synthetic oxides ( $\text{Al}_2\text{O}_3$ ,  $\text{Fe}_2\text{O}_3$  and  $\text{MnTiO}_3$ ). The HRTEM studies were performed with a Philips CM-20 scanning transmission

electron microscope (STEM) working at 200 kV (Universidad de Granada). The point to point resolution is 2.7  $\text{\AA}$  in the TEM mode and 50  $\text{\AA}$  in the STEM mode. Thin-sections prepared for TEM observation were cut perpendicular to the stretching lineation. Care was taken to limit induced deformation by excessive grinding and polishing, leaving some thin-sections thicker than the standard 30  $\mu\text{m}$ . In order to obtain the TEM specimens, Cu rings were attached to thin-sections of slates with different degrees of deformation. These rings were detached through gentle heating. Samples were further thinned with a Gatan dual ion mill. Chemical analyses of particles were made in the STEM mode with an EDAX microanalysis system. A  $200 \times 1000 \text{\AA}$  scanning area with the long axis oriented parallel to phyllosilicate packets was used for each analysis using a 50  $\text{\AA}$  beam diameter. Counting times of 200 s were used, except for Na and K that were analyzed using 30 s counting times. Albite, olivine, biotite, spessartine, muscovite, chlorite and titanite were used to obtain  $k$  factors for transformation of intensity ratios to concentration ratios.

## GEOLOGICAL SETTING AND PETROGRAPHY OF THE STUDIED MATERIALS

The study area is located in the southern part of the Central Iberian Zone (Figure 1) (Simancas *et al.*, 2001)

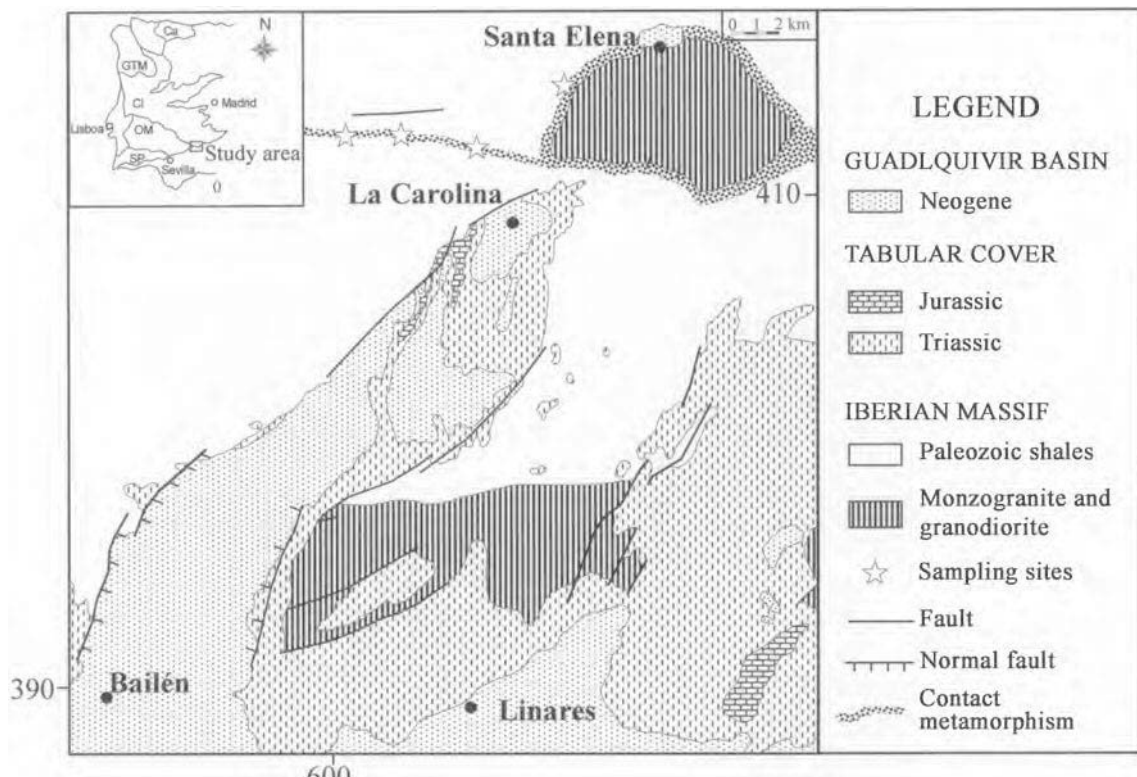


Figure 1. Geological map of the study area. SP: South Portuguese Zone; OM: Ossa Morena Zone; CI: Central-Iberian Zone; GTM: Galicia Tras os Montes Zone; WAL: Western Astur-Leonese Zone; Ca: Cantabrian Zone.

in the north of the Jaén province (SE Spain). This area is characterized by the presence of a shale- and greywacke-rich Ordovician to Lower Carboniferous sequence. Martínez Poyatos *et al.* (2001) described two phases of syn-kinematic regional very low-grade metamorphism that are related to their respective episodes of penetrative Variscan deformation in the southern Central Iberian Zone. The first phase is Devonian in age and produced high-anchizone to epizone metamorphic conditions. The second deformation is Mid Carboniferous in age and took place under late diagenesis to low-anchizone metamorphic conditions. The sequence is intruded by the Santa Elena granodioritic stock after the main phases of Variscan folding. The age of this intrusion is  $331 \pm 34$  Ma (Simancas *et al.*, 2004). A contact metamorphism aureole related to the Santa Elena stock is developed. This aureole, commonly revealed by the presence of biotite (see Figure 2) and/or andalusite, is extended in a band that appears several tens of kilometers both to the east and the west of the outcropping stock, which almost coincides with the outcrop of the Silurian succession made of black ampelitic slates. An east-west striking shear zone ~500 m wide is developed on the south border of the Santa Elena stock. The shear zone postdates the Devonian and Mid-Carboniferous metamorphism events (Jiménez-Millán *et al.*, 2003). The deformation of greatest intensity is found in the Silurian slates which are characterized by the presence of phyllonites. The shearing degree of the band shows an evolution from the north to the south. In the southern part, zones of clay gouges and sheared slates measuring few to tens of meters thick exhibit a closely-spaced sigmoidal cleavage. By contrast, black slates from the northern portion develop a weaker scaly planar-linear fabric where the sigmoidal cleavage wraps around broken andalusite crystals (see Figure 3b). No regional metamorphism

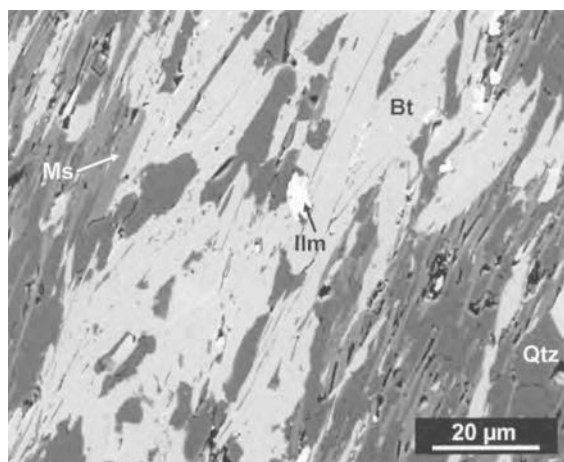


Figure 2. BSE image from an unsheared slate in the contact metamorphism aureole. Bt: biotite; Ms: muscovite; Qtz: quartz; Ilm: ilmenite.

related to the shear deformation stage has been described previously.

Optical and electron microscopy observations show that phyllosilicate minerals within the shear zone define the stretching lineation (see Figure 3), also being present in strain shadows around andalusite porphyroblasts. The phyllonites from the northern part of the shear zone are characterized by the presence of biotite, chlorite and significant amounts of muscovite. In contrast, the assemblages from the southern part are richer in Al than those of the northern part, as kaolinite is the most abundant phyllosilicate. Biotite and chlorite are commonly absent; the muscovite content is small, and some crystals of pyrophyllite appear in the southern part of the shear zone.

## CHARACTERIZATION OF THE BIOTITE GRAINS

### X-ray diffraction data

The biotite-bearing slates have XRD patterns characterized by intense 10 Å reflections due to the presence

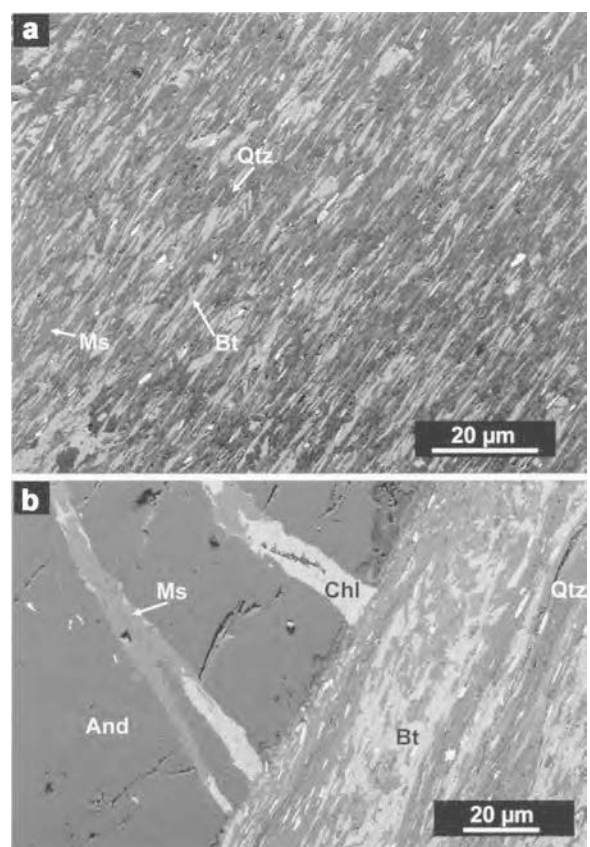


Figure 3. BSE images from a slate in the northern part of the shear zone. (a) Scaly planar-linear fabric defined by the orientation of biotite and muscovite. (b) Broken andalusite crystal inside this fabric; andalusite fractures contain muscovite and chlorite. Bt: biotite; Ms: muscovite; Chl: chlorite; And: andalusite; Qtz: quartz.

of large amounts of biotite and muscovite (Figure 4). The XRD patterns of the phyllonites from the northern part of the shear zone reveal peaks at 14.31 Å, which remain after glycolation, and a small 7.12 Å peak after dimethyl-sulfoxide treatment. These reflections are produced by chlorite, located mainly in the strain shadows and fractures of the andalusite grains.

Kaolinite appears in the clay gouges from the southern part of the shear band, with a 001 peak at 7.15 Å, which occurs at 11.2 Å after dimethyl-sulfoxide treatment and disappears after heating at 550°C.

The variety of polytypic modifications of phyllosilicates results from different possible stacking sequences of adjacent structural units. The factors controlling the

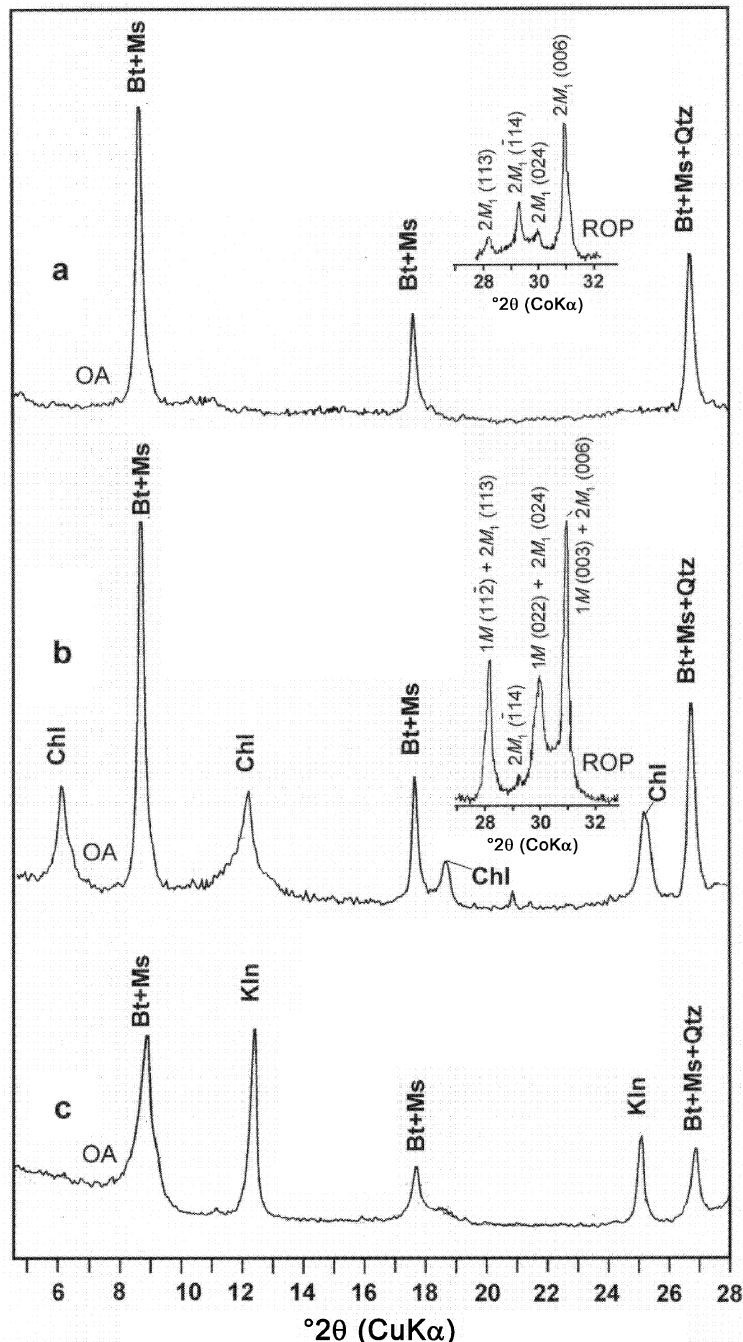


Figure 4. XRD patterns of air-dried materials: (a) unsheared sample from the contact metamorphism aureole. (b) Sample from the northern area of the shear zone. (c) Sample from the southern area of the shear zone. OA: oriented aggregates; ROP: randomly oriented powders.

crystallization of a given polytype of biotite are poorly known. The present work suggests a possible relationship between polytypism and deformation of biotites. Diffraction patterns of biotites from the study area reveal the presence of two distinct structural modifications of biotite. From six standard polytypes of micas (Smith and Yoder, 1956), the most abundant for trioctahedral micas are:  $1M > 3T \approx 2M_1$  (Bailey, 1980).  $1M$  and  $3T$  cannot be distinguished by X-ray powder diffractometry. The  $1\bar{1}\bar{2}$  ( $1M$ ) and  $\bar{1}14$  ( $2M_1$ ) diagnostic reflections make it possible to distinguish the polytypic variety of biotite. Because these diffractions are usually weak on standard powder patterns of biotite, a magnetic separator to concentrate biotite powder was used. The  $004$  reflection of chlorite coincides with the  $\bar{1}14$  reflection for  $2M_1$  biotite. Given that the presence of chlorite crystals is restricted to strain shadows and fractures of andalusite crystals, an initial handpicking of andalusite-free areas of the sample was carried out.

The presence of the  $\bar{1}14$  peak at  $3.53 \text{ \AA}$  and the low intensity of the  $113$  peak at  $3.66 \text{ \AA}$  in the XRD patterns from powders of the undeformed samples in the contact-metamorphism aureole (Figure 4a) reveal the predominance of the  $2M_1$  polytype for biotite. On the other hand, in the deformed samples from the northern area of the shear zone, the high intensity of the peaks at  $3.66 \text{ \AA}$  (corresponding to the  $1\bar{1}\bar{2}$  reflection of  $1M$  biotite and the  $113$  reflection of  $2M_1$  biotite) and  $3.40 \text{ \AA}$  (corresponding to the  $022$  reflection of  $1M$  biotite and the  $024$  reflection of the  $2M_1$  biotite) and the presence of a low-intensity reflection at  $3.53 \text{ \AA}$  ( $2M_1$  biotite) indicate that although  $2M_1$  polytype is present, the  $1M$  polytype is predominant (Figure 4b).

#### *Biotite from unsheared slates in the contact-metamorphism aureole*

Biotite plates from unsheared slates are aligned parallel to the main schistosity, although biotite grains with other orientations are also present (Figure 2). Back-scattered electron (BSE) images are homogeneous, suggesting the absence of intergrowth with other minerals. The EMPA results for these biotite grains are also very homogeneous. Biotite analyses are characterized by a very slight deficit in the interlayer charge (Table 1). They also show slightly low totals and high Ti contents, as are commonly reported in analyses of metamorphic biotite (Guidotti, 1984).

Low-magnification TEM images obtained from contact-metamorphosed slates unaffected by the shear zone show that biotite grains occur as parallel or subparallel domains ranging up to  $1 \mu\text{m}$  in thickness (Figure 5a). Lattice fringes are straight, have uniform contrast and are continuous over hundreds of  $\text{\AA}$  (Figures 5b and e). Most of the biotite packets appear defect free although locally some dislocation cores can be observed. Selected area electron diffraction patterns along one of the directions  $<100>$ ,  $<110>$  and  $<1\bar{1}0>$  show intense

reflections with little diffuseness and minor streaking along  $c^*$  (Figure 5c,d). These zone axes cannot be distinguished due to the defective character of the biotite samples and hereafter such directions are expressed as  $<100>/<110>/<1\bar{1}0>$ . Periodic non- $00l$  reflections with  $20 \text{ \AA}$  periodicity are observed corresponding to a two-layer polytype, probably  $2M_1$ , taking into account XRD data. The AEM data show that this biotite is K-rich ( $\sim 0.80$  atoms per formula unit), with high interlayer charge. The biotite from these samples is quite homogeneous, and we observed no important alteration effects such as chlorite-rich regions or Fe-rich amorphous regions associated with the biotite–chlorite transformation. Biotite crystals are locally affected by layer bending and deformation.

#### *Deformed biotites from the north area of the shear zone*

Biotite grains from the northern area of the shear zone appear as very elongate thin mica fishes. They are usually oriented with their long axes parallel or at a small angle to the shearing foliation (Figures 3a and b). The BSE images do not reveal intergrowth with other minerals but EMPA data indicate a wide compositional variability (Table 1). A mica phase very similar to the unsheared biotite was identified. In addition, EMP analyses yielded compositions that were Fe- and Mg-enriched but poor in Si, Ti and alkali elements, which

Table 1. EMPA analyses of biotite in the shear zone. Structural formulae adjusted to  $O_{10}(OH)_2$ .

	1	2	3	4	5	6
$SiO_2$	35.01	34.95	35.50	35.42	31.44	31.55
$TiO_2$	1.62	1.66	1.56	1.68	0.81	0.94
$Al_2O_3$	20.71	20.68	21.01	20.82	21.49	20.26
$FeO$	19.28	19.12	18.67	19.02	21.79	22.73
$MnO$	0.10	0.10	0.12	0.09	0.12	0.11
$MgO$	7.52	7.47	7.45	7.58	8.97	9.28
$CaO$	0.00	0.00	0.02	0.00	0.02	0.01
$Na_2O$	0.26	0.19	0.32	0.23	0.05	0.08
$K_2O$	8.34	8.42	8.54	8.46	5.85	5.66
Total	92.84	92.59	93.19	93.30	90.54	90.62
Si	2.711	2.713	2.729	2.723	2.514	2.534
Ti	0.094	0.097	0.090	0.097	0.049	0.057
Al	1.890	1.892	1.904	1.887	2.025	1.918
$Fe^{2+}$	1.248	1.241	1.200	1.223	1.457	1.526
$Mn^{2+}$	0.007	0.007	0.008	0.006	0.008	0.008
Mg	0.868	0.864	0.854	0.869	1.069	1.111
Ca	0.000	0.000	0.002	0.000	0.001	0.001
Na	0.039	0.029	0.048	0.034	0.008	0.013
K	0.824	0.834	0.838	0.830	0.597	0.580
$\Sigma cat$	7.681	7.676	7.672	7.668	7.727	7.746

1 and 2: biotite from unsheared slates in the contact-metamorphism aureole.

3 and 4: biotite from the northern area of the shear zone.

5 and 6: biotite from the northern area of the shear zone showing some chlorite contamination.

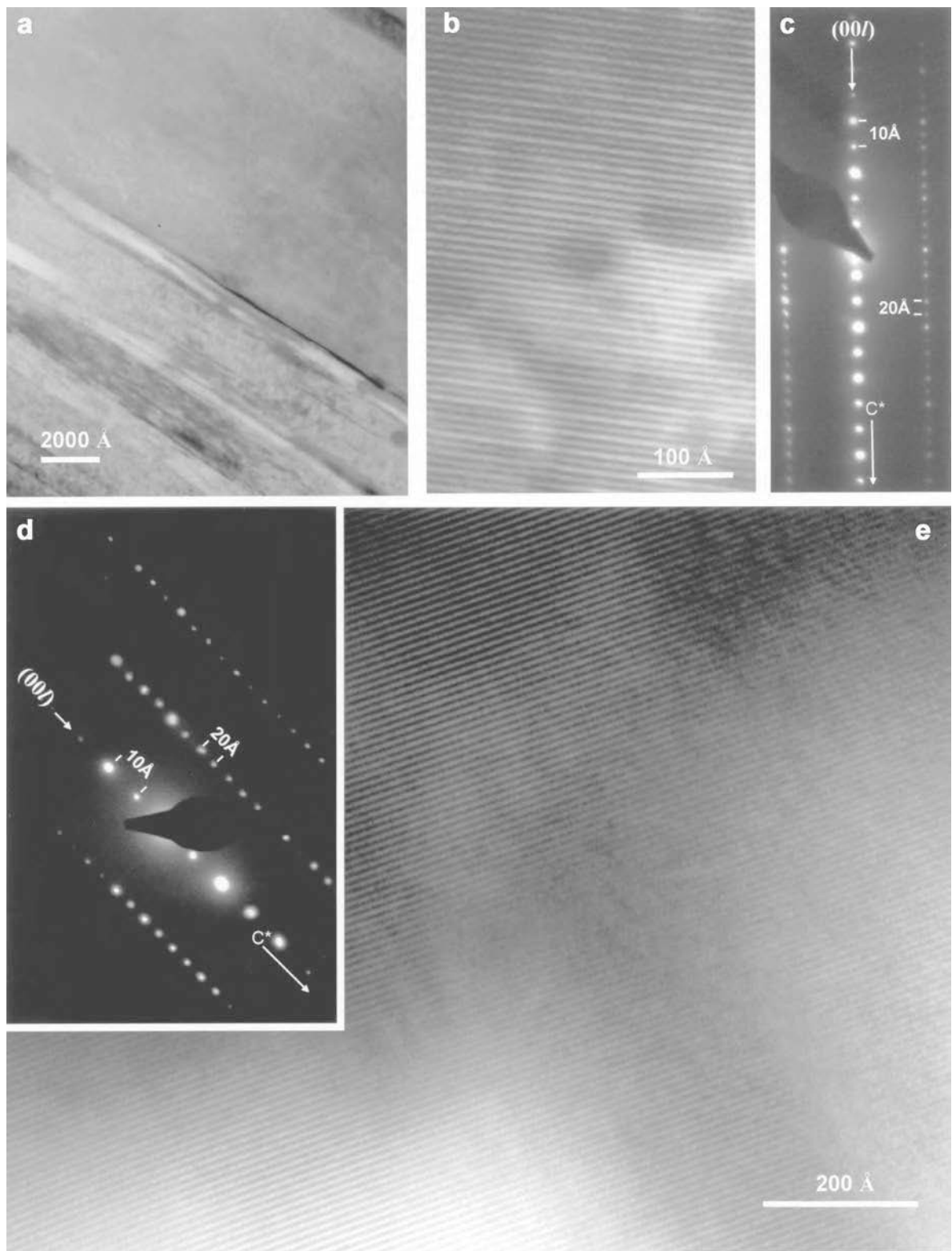


Figure 5. TEM images from contact-metamorphosed slates unaffected by the shear zone. (a) Low-magnification image showing biotite grains with sub-parallel packets. (b) Lattice-fringe image of a part of this biotite crystal. (c,d) SAED images recorded along  $\langle 100 \rangle / \langle 110 \rangle / \langle 1\bar{1}0 \rangle$  showing non-00l reflections with 20 Å periodicity. (e) Lattice-fringe image corresponding to SAED images shown in parts c and d.

can be interpreted as intermediate between biotite and chlorite, rather than proper biotite.

The biotite grains in the northern area of the shear zone are characterized by the presence of numerous elongated gaps in low-magnification TEM images. The biotite packets display a mottled appearance consisting of blocky patches and irregular areas of darker contrast (Figure 6a). Mottling distribution is oblique to (001) biotite basal planes.

The SAED patterns of biotite crystals obtained from sheared samples display high orders of 00*l* reflections with  $d_{001}$  of 10 Å (Figures 6b,c and 7b). Most of the SAED patterns obtained from these biotite grains show diffuse streaking along  $c^*$ . Diffuseness normal to  $c^*$  is sometimes observed, which can be caused by small variations in the orientation of biotite packets. Non-00*l* reflections are ill-defined and non-periodic along  $c^*$ , and diffuse parallel to  $c^*$ , indicating that stacking is partially random. Such SAED patterns have commonly been

labeled as being diagnostic of  $1M_d$  polytypism. Lattice-fringe images show alternation of regions with high and low dislocation densities (Figures 6b, 6c, 6d, 7a and 7c).

This biotite is commonly characterized by structural defects and the interlayering of chlorite. Although dislocations are the most common defects found, other shear-strain structures such as voids and low-angle boundaries are also observed. Figure 6d shows that the dislocations perturb the biotite layering. Lattice fringes are commonly curved, suggesting variability in the  $d_{001}$  value. In some cases, the (001) layers show complex folding and they are disrupted. Figure 6d shows that the biotite grains from this zone contain straight microcavities, associated with the presence of dislocations. In some of the microvoids produced by the structural defects, ~5 Å lattice fringes can be observed (Figure 6d). Figure 6e shows 5 Å lattice fringes in a microvoid from a thin area of the TEM specimen forming a small angle with biotite layers, suggesting

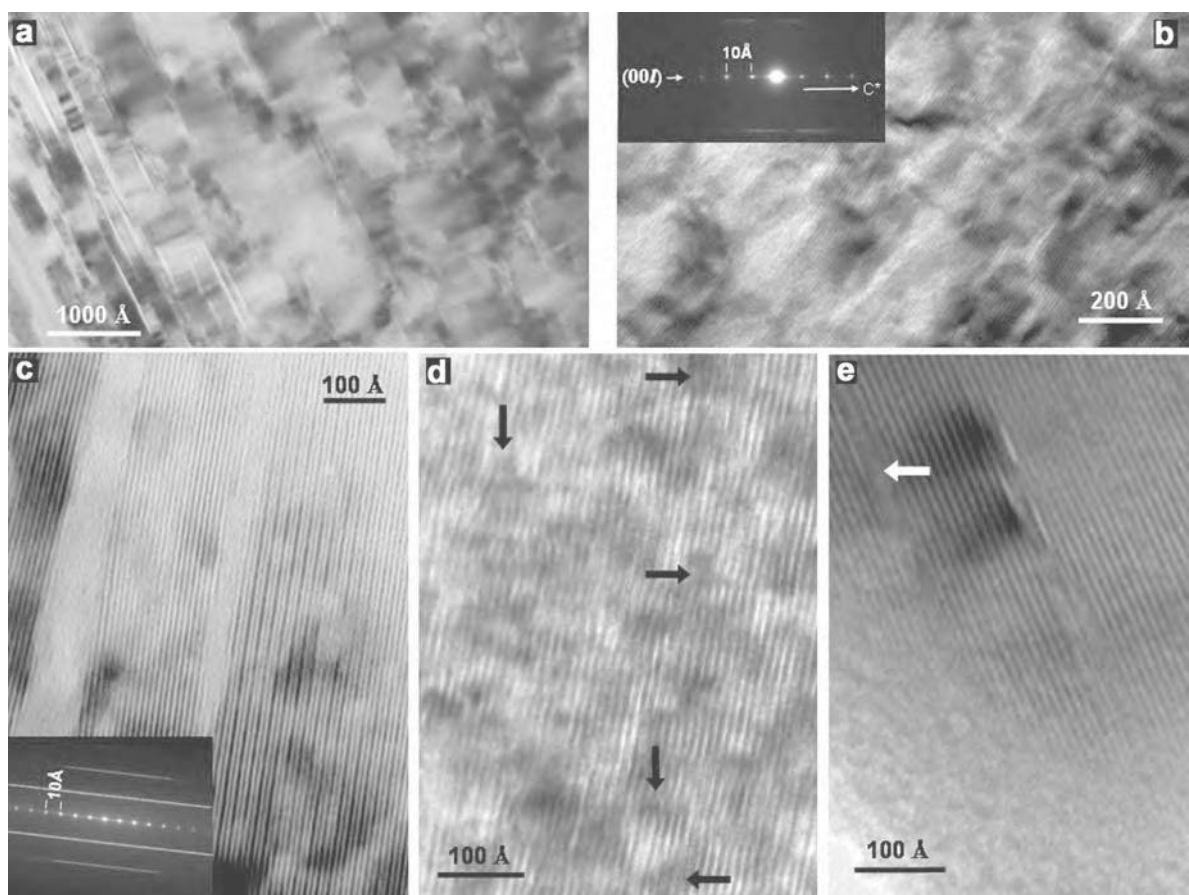


Figure 6. TEM images from slates in the northern area of the shear zone. (a) Mottling in the biotite packets. (b,c) HRTEM and SAED images obtained from these packets. HRTEM and SAED images in b are recorded along  $<100>/<110>/<1\bar{1}0>$ . The SAED pattern shows that non-00*l* reflections are non-periodic along  $c^*$ . The SAED pattern in c shows significant disorder. (d) Defect-rich packets of biotite with curved lattice fringes, disrupted layering and microvoids associated to dislocations that contain ~5 Å lattice fringes (arrows). (e) 5 Å lattice fringes (arrow) in a microvoid from a thin area of the TEM specimen forming a small angle with the biotite layers.

the 5 Å layers do not appear from off-set of TOT layers. Moreover, these defect-rich packets are characterized by an excess of Fe and Mg, and a deficiency of Si and Al, as shown by the AEM analyses (Table 2), which suggest that the ~5 Å lattice-fringe regions probably correspond to brucite-like sheets.

Some biotite crystals show areas parallel to the (001) cleavage planes where the frequency of chlorite interlayering is high (Figure 7a). Quite large (up to 200–500 Å thick) flakes of chlorite (with regular sequences of 14 Å layers) also occur locally. The TEM images show that some packets of 14 Å chlorite layers are locally interstratified with a 7 Å layer phase. Lateral changes between 7 Å and 14 Å layers can be observed. The SAED pattern in Figure 7B showing 00l reflections with 7 Å periodicities suggests the existence of berthierine-like layers intergrown with the biotite crystals. Lattice-fringe images corresponding to this SAED pattern reveal that some areas of the biotite crystals contain packets of 7 Å layers whose thicknesses range between 50 and 200 Å (Figure 7c).

Figure 7a shows berthierine-chlorite interfaces viewed along the <100> direction. Apparently unstrained contacts between berthierine and chlorite are clearly visible. These results are similar to those of Xu and Veblen (1996), where no significant strain is evident at the interfaces. Table 2 shows that chlorite is Fe rich (up to 2.54 atoms p.f.u.) and that AEM data of

the 14 Å, 7 Å and (14 + 7) Å areas show lack of systematic differences in chemical compositions between both phyllosilicates.

#### *Kaolinized biotite in the clay gouges from the southern part of the shear zone*

Optical, SEM and EMPA studies did not reveal the presence of biotite grains in the clay gouges from the highly deformed materials in the southern part of the shear zone, where kaolinite is the predominant phyllosilicate. However, the TEM study showed thin packets (<100 Å) with 10 Å fringes interlayered with electron beam-damaged areas (Figure 8). The AEM data from these regions are Al rich but their large Fe, Mg and Ti contents suggest the presence of kaolinite intergrown with relics of biotite (Table 2).

## DISCUSSION

#### *Evolution of the metamorphic conditions during shearing*

The petrography of the sheared materials suggests that the deformational episode associated with tensional stresses of a tectonic event that post-dated the intrusion of the Santa Elena stock and the Devonian and mid-Carboniferous metamorphism events produced the elongation, rotation and partitioning of the andalusite, and biotite crystallized during the contact-metamorphism

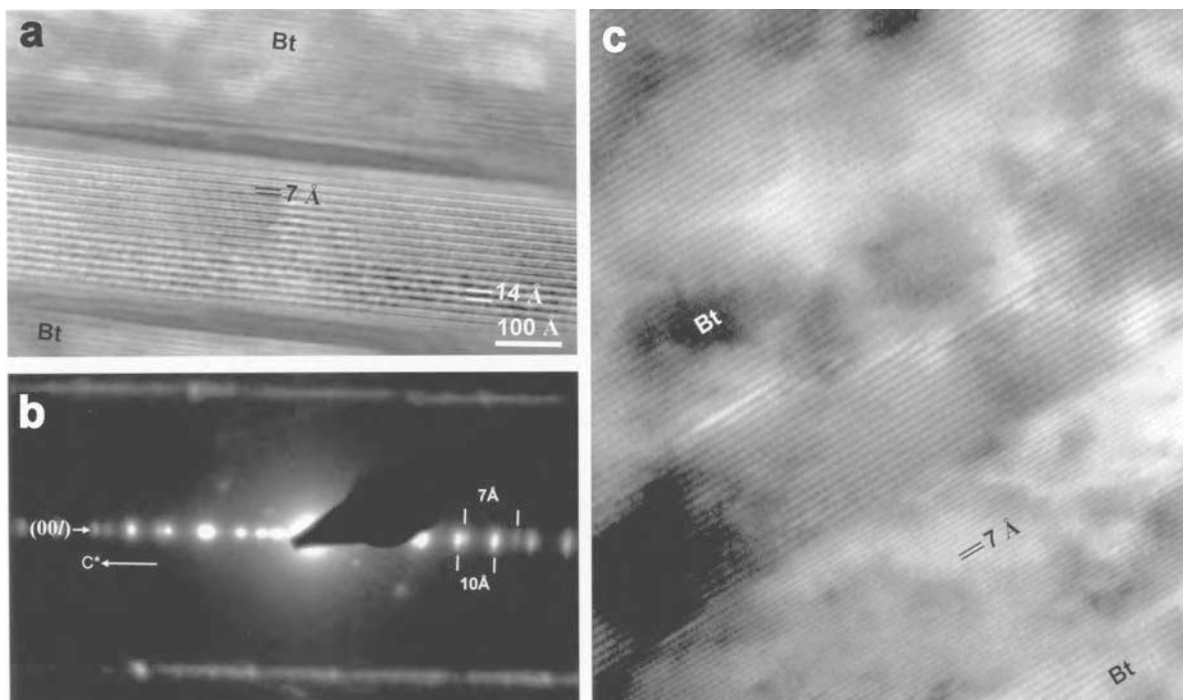


Figure 7. (a) Biotite packets with chlorite interlayering parallel to the (001) cleavage planes. The chlorite packet shows interlayering and lateral changes of 14 Å and 7 Å layers. (b) SAED pattern showing parallel 00l reflections of 7 and 10 Å periodicities. (c) Corresponding lattice fringe image of biotite with parallel intergrown of 7 Å phase packet. HRTEM and SAED images in parts b and c are recorded along <100>/<110>/<110>. All the images are taken from slates in the northern area of the shear zone. Bt: biotite.

Table 2. AEM analyses of biotite and chlorite in the study area.

Analysis	1	2	3	4	5	6	7	8	9
Si	2.72	2.72	2.65	2.66	2.56	2.56	2.50	2.94	2.98
Ti	0.10	0.10	0.09	0.09	0.00	0.01	0.00	0.05	0.05
Al	1.91	1.88	1.84	1.85	3.00	3.00	3.06	2.64	2.61
Fe	1.22	1.25	1.39	1.38	2.48	2.49	2.54	0.47	0.46
Mg	0.86	0.86	1.01	1.00	1.87	1.87	1.84	0.42	0.42
Na	0.05	0.05	0.00	0.00	0.00	0.00	0.00	0.00	0.00
K	0.79	0.80	0.69	0.69	0.00	0.00	0.00	0.31	0.27

1 and 2: structural formulae for unsheared biotite normalized to  $O_{10}(OH)_2$ ; 3 and 4: structural formulae for defect-rich biotite normalized to  $O_{10}(OH)_2$ ; 5 to 7: structural formulae for chlorite normalized to  $O_{10}(OH)_8$ ; 8 and 9: AEM analyses of biotite relics mixed up with kaolinite, normalized to  $O_{10}(OH)_2$

stage produced by the Santa Elena stock intrusion. The crystallization in the northern part of the shear band of chlorite and muscovite filling the strain shadows and fractures of the broken andalusite crystals, as well as the presence of pyrophyllite reliefs in the southern part of this band suggest a first stage of deformation under higher-temperature conditions ( $>\sim 270\text{--}290^\circ\text{C}$ , according to Parry, 1998). The later alteration of chlorite, andalusite and muscovite to kaolinite indicates a second stage under lower-temperature conditions.

#### *Structural defects and polytype as a function of the deformation*

The XRD and TEM data indicate that the two-layer polytype (probably  $2M_1$ ) is the most common structure in the biotite crystals from the contact-metamorphosed slates that were not affected by shearing. This polytype is very common in slightly deformed biotite grains with a low dislocation density (Bell and Wilson, 1981). Figure 5c,d shows that the streaking in this biotite is weak. The absence of streaking along  $c^*$  indicates the absence of stacking disorder.

Under applied stress, deformation and shearing cause the development of dislocations, which can develop stacking disorder. The dislocation density increases with increasing strain. Streaking occurs if there is a high

density of stacking disorder, indicating that high strains were achieved (Bell and Wilson, 1981). In the deformed biotite from the shear zone, XRD and TEM data suggest that the disordered polytype ( $1M_d$ ) is predominant. Moreover, the degree of streaking or stacking disorder is more pronounced for the disordered polytype than for the two-layer polytype. Given that the degree of streaking is an indication of the intensity of deformation, the disordered polytype packets are more deformed than the two-layer polytype packets. These data suggest that the disordered polytype was formed by deformation from the two-layer polytype.

#### *The influence of structural defects on the retrograde chloritization*

The HRTEM images and AEM-EPMA analytical data reveal that the chemical modification of the biotite grains is strongly associated with the microtextural evidence of deformation. Thus, packets rich in defects, that appear to consist of brucite-like sheets in microvoids associated with dislocations, are characterized by an excess of Fe and Mg, and a deficiency of Si, Al and alkalis. Active deformation can enhance the diffusion process within the biotite grains promoting metamorphic reactions. The diffusion mechanisms can be affected by the introduction of lattice defects and the development of microcavities allowing a fluid to permeate and effectively permit transport processes to operate (Bell and Cuff, 1989). We consider that the microcavities observed in the biotite grains from the shear zone can act as potential channels for transport of fluids and serve as sites for chloritization of biotite (Olives *et al.*, 1983). Therefore, we suggest that the occurrence of chlorite-berthierine domains within biotite is probably related to retrograde metamorphism, along micro-cavities that formed during shearing. Lattice fringes in TEM images of microvoids, showing that brucite-like and biotite (001) layers are not completely parallel with respect to each other, suggest that dissolution-precipitation was the predominant reaction mechanism rather than replacement of interlayer or tetrahedral sheets of biotite. However, the existence of micro-cavities may be due

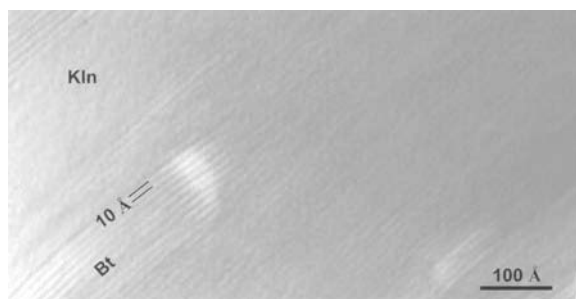


Figure 8. HRTEM image of a thin packet with 10 Å fringes (biotite) interlayered with electron beam damaged areas (kaolinite). Bt: Biotite. Kln: Kaolinite.

to the volume decrease from biotite to chlorite *via* the formation mechanism suggested by Veblen and Ferry (1983) precluding any unambiguous identification of the transformation mechanisms based on TEM images.

The AEM analyses of the 14 Å, 7 Å and (14 + 7) Å areas show a lack of systematic differences in chemical compositions between both chlorite and berthierine and they can be considered as true polymorphs. The contacts between chlorite and berthierine are free of other phases, strain or microvoids, which indicates that the transformation was isochemical and at constant volume. Berthierine is replaced by chlorite with along-layer transitions as is consistent with a direct replacement mechanism. Therefore, these data indicate that chlorite is the final product of alteration of biotite, with berthierine as an intermediate metastable phase. Abad-Ortega and Nieto (1995) showed that berthierine is metastable compared to chlorite during the alteration of cordierite.

In the strongly deformed clay gouges from the southern part of the shear zone, the retrogression was more intense, producing the phyllosilicate replacement by kaolinite.

## CONCLUSIONS

Combined mineralogical, petrological and tectonic studies performed on the biotite-bearing slates in a contact metamorphism aureole affected by a shear band have allowed the detection of several effects of magmatic, metamorphic, tectonic and fluid-rock interaction processes that occurred after the main phases of Variscan folding in the Southern Iberian Massif.  $2M_1$  biotite was crystallized during the contact-metamorphism stage produced by the Santa Elena stock intrusion. The shear band developed on the contact metamorphism aureole produced the rotation and elongation of the biotite crystals defining the stretching lineation of the sheared slates. An initial synkinematic retrograde metamorphic stage produced during the shearing event caused the crystallization of chlorite, muscovite and pyrophyllite. The shearing process evolved towards progressively cooler conditions producing a retrograde event characterized by the kaolinite crystallization. Deformation and fluid-rock interaction processes produced structural and chemical modifications of the biotite crystals from the shear band. In this biotite, deformation is responsible for the high dislocation density, the presence of microvoids, the predominance of a disordered polytype ( $1M_d$ ) and the streaking of the SAED patterns. Furthermore, microcavities favored the fluid-mineral interaction processes allowing the beginning of the chloritization with the formation of berthierine as an intermediate metastable phase finally replaced by chlorite. In the strongly deformed areas of the shear zone, the intense fluid-rock interaction under cooler conditions produced the kaolinitization of the

'pre-existing' phyllosilicates, preventing the chloritization of biotite.

## ACKNOWLEDGMENTS

We would like to thank M.M. Abad (CIC, Univ. Granada) for her help with the HRTEM work. We are also grateful to P. Heaney and two anonymous reviewers for their helpful comments and suggestions. Financial support was provided by Research Project BTE2003-07867-C02 (Spanish Ministry of Science and Technology) the Research Groups RNM-179 and RNM-325 of the Junta de Andalucía. We are grateful to Nick Snow for his assistance with the English.

## REFERENCES

- Abad-Ortega, M.M. and Nieto, F. (1995) Genetic and chemical relationships between berthierine, chlorite and cordierite in nodules associated to granitic pegmatites of Sierra-Albarrana (Iberian Massif, Spain). *Contributions to Mineralogy and Petrology*, **120**, 327–336.
- Bailey, S.W. (1980) Structures of layer silicates. Pp. 1–125 in: *Crystal Structures of Clay Minerals and their X-ray Identification* (G.W. Brindley and G. Brown, editors). Monographs **5**. Mineralogical Society, London.
- Bell, I.A. and Wilson, C.J.L. (1981) Deformation of biotite and muscovite; TEM microstructure and deformation model. *Tectonophysics*, **78**, 201–228.
- Bell, T.H. and Cuff, C. (1989) Dissolution, solution transfer, diffusion versus fluid flow and volume loss during deformation metamorphism. *Journal of Metamorphic Geology*, **7**, 425–447.
- Christoffersen, R. and Kronenberg, A.K. (1993) Dislocation interactions in experimentally deformed biotite. *Journal of Structural Geology*, **15**, 1077–1095.
- Guidotti, C.V. (1984) Micas in metamorphic rocks. Pp. 357–368 in: *Micas* (S.W. Bailey editor). Reviews in Mineralogy, **13**. Mineralogical Society of America, Washington D.C.
- Iijima, S. and Zhu, J. (1982) Muscovite-biotite interface studied by electron microscopy. *American Mineralogist*, **67**, 1195–1205.
- Jiménez-Millán, J., Vázquez, M., Nieto, F., Velilla, N., Azor, A., Martínez-Poyatos, D.J. and Martín-Parra, L.M. (2003) Effects on phyllosilicates of successive contact metamorphism, tectonic shear strain and hydrothermal processes in the Southern Domain of the Central Iberian Zone, Iberian Massif, Spain. Pp 142–143 in: *Abstract Book of Euroclay 2003* (M.F. Brigatti, editor). Modena, Italy.
- Kogure, T. and Banfield, J.F. (2000) New insights into the mechanism for chloritization of biotite using polytype analysis. *American Mineralogist*, **85**, 1202–1208.
- Kronenberg, A.K., Kirby, S.H. and Pinkston, J. (1990) Basal slip and mechanical anisotropy of biotite. *Journal of Geophysical Research*, **95**, B12, 19257–19278.
- Martínez-Poyatos, D., Nieto, F., Azor, A., Simancas, J.F. (2001) Relationships between very low-grade metamorphism and tectonic deformation: examples from the southern Central Iberian Zone (Iberian Massif, Variscan Belt). *Journal of the Geological Society*, **158**, 953–968.
- Noe, D.C., LaVan, D.A. and Veblen, D. (1999) Lap shear testing of biotite and phlogopite crystals and the application of interferometric strain/displacement gages to mineralogy. *Journal of Geophysical Research*, **104**, B8, 17811–17822.
- Olivés, J. and Amouric, M. (1983) Biotite chloritization by interlayer brucitization, as seen by High-Resolution Transmission Electron-Microscopy. *Fortschritte der Mineralogie*, **61**, 162.

- Olives, J., Amouric, M., Fouquet, C.D. and Baronnet, A. (1983) Interlayering and interlayer slip in biotite as seen by HRTEM. *American Mineralogist*, **68**, 754–758.
- Ooteman, A., Ferrow, E.A. and Lindh, A. (2003) An electron microscopy study of deformation microstructures in granitic mylonites from southwestern Sweden, with special emphasis on the micas. *Mineralogy and Petrology*, **78**, 255–268.
- Parry, W.T. (1998) Fault-fluid compositions from fluid-inclusion observations and solubilities of fracture-sealing minerals. *Tectonophysics*, **290**, 1–26.
- Sanchez-Navas, A. and Galindo-Zaldívar, J. (1993) Alteration and deformation microstructures of biotite from plagioclase-rich dykes (Ronda Massif, S-Spain). *European Journal of Mineralogy*, **5**, 245–256.
- Simancas, J.F., Exposito, I., Azor, A., Poyatos, D.M. and Lodeiro, F.G. (2004) From the Cadomian orogenesis to the Early Palaeozoic Variscan rifting in Southwest Iberia. *Journal of Iberian Geology*, **30**, 53–71.
- Simancas, J.F., Poyatos, D.M., Exposito, I., Azor, A. and Lodeiro F.G. (2001) The structure of a major suture zone in the SW Iberian Massif: the Ossa-Morena/Central Iberian contact. *Tectonophysics*, **332**, 295–308.
- Smith, J.V. and Yoder, H.S. (1956) Experimental and theoretical studies of the mica polymorphs. *Mineralogical Magazine*, **31**, 209–235.
- Veblen, D.R. and Ferry, J.M. (1983) A TEM study of the biotite chlorite reaction and comparison with petrologic observations. *American Mineralogist*, **68**, 1160–1168.
- Xu, H.F. and Veblen, D.R. (1996) Interstratification and other reaction microstructures in the chlorite-berthierine series. *Contributions to Mineralogy and Petrology*, **124**, 291–301.

(Received 7 February 2006; revised 29 January 2007;  
Ms. 1138 ; A.E. Peter J. Heaney)